

Cell size, mechanical tension, and GTPase signaling in the Single Cell

Andreas Buttenschön · Yue Liu · Leah Edelstein-Keshet

Received: date / Accepted: date

Abstract Cell polarization requires redistribution of specific proteins to the nascent front and back of a eukaryotic cell. Among these proteins are Rac and Rho, members of the small GTPase family that regulate the actin cytoskeleton. Rac promotes actin assembly and protrusion of the front edge, whereas Rho activates myosin-driven contraction at the back. Mathematical models of cell polarization at many levels of detail have appeared. One of the simplest based on “wave-pinning”, consists of a pair of reaction-diffusion equations for a single GTPase. Mathematical analysis of wave-pinning so far is largely restricted to static domains in one spatial dimension. Here we extend the analysis to cells that change in size, showing that both shrinking and growing cells can lose polarity. We further consider the feedback between mechanical tension, GTPase activation, and cell deformation in both static, growing, shrinking, and moving cells. Special cases (spatially uniform cell chemistry, absence or presence of mechanical feedback) are analyzed, and the full model is explored by simulations in 1D. We find a variety of novel behaviors, including “dilution-induced” oscillations of Rac activity and cell size, as well as gain or loss of polarization and motility in the model cell.

Keywords Cell size, motility, GTPases, Rac and Rho, cell polarization, reaction-diffusion equations, growing 1D domain

Acknowledgements LEK and coauthored are (partially) supported by NSERC (Natural Sciences and Engineering Research Council) Discovery grant 41870 to LEK. YL was partially supported by an NSERC postgraduate fellowship. AB was partially supported by an NSERC PDF Fellowship. We are grateful to the Pacific Institute for Mathematical Sciences for providing space and resources for AB’s postdoctoral research. The authors thank C. Zmurchok and W. R. Holmes and E. Rens for valuable discussions.

A. Buttenschön
Department of Mathematics, University of British Columbia, Vancouver V6T 1Z2, BC, Canada
E-mail: abuttens@math.ubc.ca

Y. Liu
Department of Mathematics, University of British Columbia, Vancouver V6T 1Z2, BC, Canada
E-mail: liuyue@math.ubc.ca

L. Edelstein-Keshet
Department of Mathematics, University of British Columbia, Vancouver V6T 1Z2, BC, Canada
E-mail: keshet@math.ubc.ca

1 Introduction

Cell polarization and motility play a vital role in living organisms across all size scales. In normal development, wound healing, and immune surveillance, cells undergo directed migration tightly controlled by intracellular signaling pathways. Hence, these cellular phenomena have attracted attention of modelers, and gained representation at a whole spectrum of levels of detail, in 1D (Otsuji et al. 2007; Mori et al. 2008; Dawes and Edelstein-Keshet 2007; Holmes et al. 2012), 1.5D (the edge of a 2D domain) (Meinhardt 1999; Neilson et al. 2011), as well as 2D (Marée et al. 2006; Wolgemuth and Zajac 2010; Marée et al. 2012; Camley et al. 2013), and 3D (Cusceddu et al. 2018) geometries.

An elementary model for cell polarization by “wave-pinning” was introduced in (Mori et al. 2008) in 1D, based on a single signaling protein (GTPase) inside a stationary cell of fixed length. The wave-pinning model was a simplification of the more biologically detailed models of GTPase role in polarity captured in (Marée et al. 2012; Jilkin and Edelstein-Keshet 2011). Generalization of this model to a pair of mutually antagonistic (Rac-Rho) GTPases and use of approximation methods demonstrated coexistence of cell states such as polarized, low uniform and high uniform protein activity levels (Holmes and Edelstein-Keshet 2016).

As interesting aspect of the GTPases Rac and Rho is that they tend to concentrate at cell edges, where they drive actin assembly and edge protrusion (Rac) or actomyosin contraction (Rho), which moves the cell edge outwards or inwards. The cell tends to resist deformation, which means that when one edge moves, the opposite edge is pulled or pushed accordingly. At the same time, protrusion or retraction may cause cell volume to change, particularly in combination with aquaporin channels that allow water to flow in or out of the cell. Hence, cells can undergo fluctuations in size (Zehnder et al. 2015) that potentially affect their internal concentration.

In (Mori et al. 2008, 2011; Jilkin and Edelstein-Keshet 2011; Holmes and Edelstein-Keshet 2016), cell size was assumed to be static, whereas here we lift this restriction. The effect of cell size was briefly considered in modeling the polarization response of HeLa cells to Rac stimulation in microfluidic channels (Holmes et al. 2012). It is also incorporated in a companion paper by (Zmurchok and Holmes 2019), where the focus is on cell shape diversity arising from autoactivation as well as mutual inhibition in Rac-Rho interactions. Cells were deformable in (Zmurchok et al. 2018), but possibility dilution was neglected, whereas here we consider such effect. Finally, in (Zmurchok et al. 2018; Bui et al. 2019), feedback from tension due to cell deformation was included, but only in model cells with spatially uniform GTPase activity. Here we generalize to full spatially distributed GTPase activity, which introduces new interesting behavior.

Mathematical analysis is possible for simple geometries and models with few components, and becomes increasingly forbidding as the size of the signaling network or the complexity of the geometry increases. For this reason, we concentrate on a toy model in 1D geometry to describe the interplay between cell size, cell polarization/motility and mechanical feedback. We show that this interplay can lead to cycles of expansion and contraction in certain cases and/or initiation of motility after some delay time.

The model is simple enough that some analytical results can be written to characterize regimes of behaviour. We can apply several methods, including linear stability analysis, approximations of kinetic terms by piecewise linear functions (where steady states can be found in closed form), as well as bifurcation analysis and numerical PDE solutions. Using these methods, we here generalize and extend some of the previous mathematical findings about wave-pinning, and help to increase insight about how such mechanisms for cell polarization could operate.

2 Preexisting model to be generalized

We briefly outline previous work (Mori et al. 2008; Holmes and Edelstein-Keshet 2016) as a starting point for our paper. Concentrations of active (G) and inactive (G_i) GTPases are modeled by reaction-diffusion

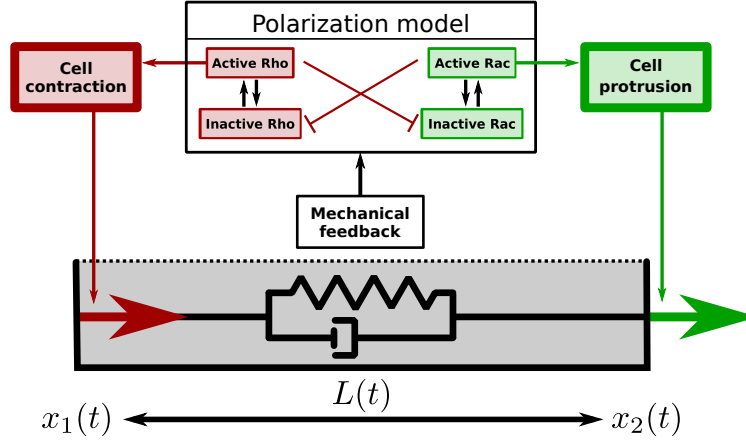


Fig. 1 The model considered here has two key modules: the polarization model, and the one-dimensional visco-elastic cell model. Here a Kelvin-Voigt element is placed between the cell endpoints ($x_1(t)$ and $x_2(t)$). While other visco-elastic models are possible, here we focus on the interplay between mechanics and signalling. The polarization model captures the spatio-temporal dynamics of one or more small GTPases affecting the cell's cytoskeleton. Here their effects i.e. assembly of cell protrusions (Rac) or cell contractions (Rho) are captured by applying forces on the cell's endpoints. Here we consider three different signalling modules. For a spatially uniform single GTPase module (either Rac or Rho) we present detailed phase-plane and bifurcation analysis in Section 7. In particular, we demonstrate the existence of “dilution-induced” oscillations of Rac concentration and cell size. In Section 8 we show that a spatially heterogeneous GTPase (Rac or Rho) allows the cell to polarize and move. However, if a cell is too soft i.e. it undergoes large size changes, it may undergo “dilution-induced” depolarize. Finally, in Section 8.2 we consider a polarization module consisting of antagonistic Rac and Rho. We capture all features of the single GTPase models, but also gain more complicated spatio-temporal patterns.

(RD) equations,

$$\begin{aligned} G_t &= D\Delta G + A(G)G_i - IG, \\ (G_i)_t &= D_i\Delta G_i - A(G)G_i + IG. \end{aligned} \quad (1)$$

Active GTPase is membrane-bound, so the rates of diffusion satisfy $D \ll D_i$. $A(G)$ is a rate of activation and I a rate of inactivation. Feedback from the active GTPase to its kinetics is assumed to be directed through the rate of activation of GTPase by GEFs (guanine nucleotide exchange factors), whereas the rate of inactivation by GAPs (GTPase activating proteins) is taken as constant. Since the GTPase cannot enter or leave through the cell edge, the PDEs are supplemented by Neumann (no-flux) boundary conditions. Equations (1) conserve the total amount of GTPase (G_T) in a cell, that is

$$G_T := \int (G + G_i) \, dx.$$

As in previous papers, we consider both the single GTPase (“wave-pinning”) model of (Mori et al. 2008), as well as the Rac-Rho model of (Holmes and Edelstein-Keshet 2016).

Single GTPase model: The standard functional form for the rate of activation, $A(G)$, is

$$A(G) = \left(\beta + \gamma \frac{G^n}{1 + G^n} \right).$$

The Rac-Rho (two GTPase) model: Let G_R, G_ρ represent the activities of Rac and Rho GTPases, respectively. We assume mutual inhibition. That is, the rate of activation of Rac is reduced by Rho and vice versa. The standard function form for the activation rate of Rac is

$$A_R(G_\rho) = \left(\beta + \gamma \frac{1}{1 + G_\rho^n} \right).$$

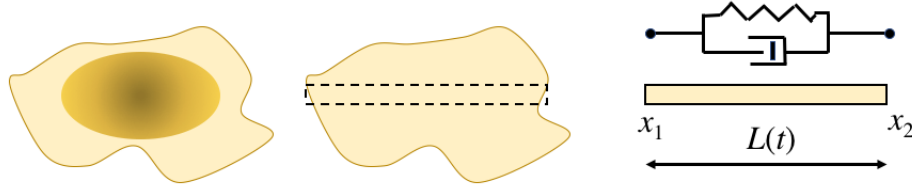


Fig. 2 Left: Top-down view of a eukaryotic cell. Middle: the nucleus has been removed, so that the cell fragment is a thin sheet with approximately uniform thickness ($< 1\mu\text{m}$). A 1D transect across the cell is shown. Right: the front and rear positions of the cell edge are labeled. We consider cell motion such that x_1, x_2, L are all possibly time-dependent. The region $x_1 \leq x \leq x_2$ is the domain inside which GTPase reaction-diffusion takes place. Mechanically, the 1D cell is represented as a spring dashpot (Kelvin-Voigt) element.

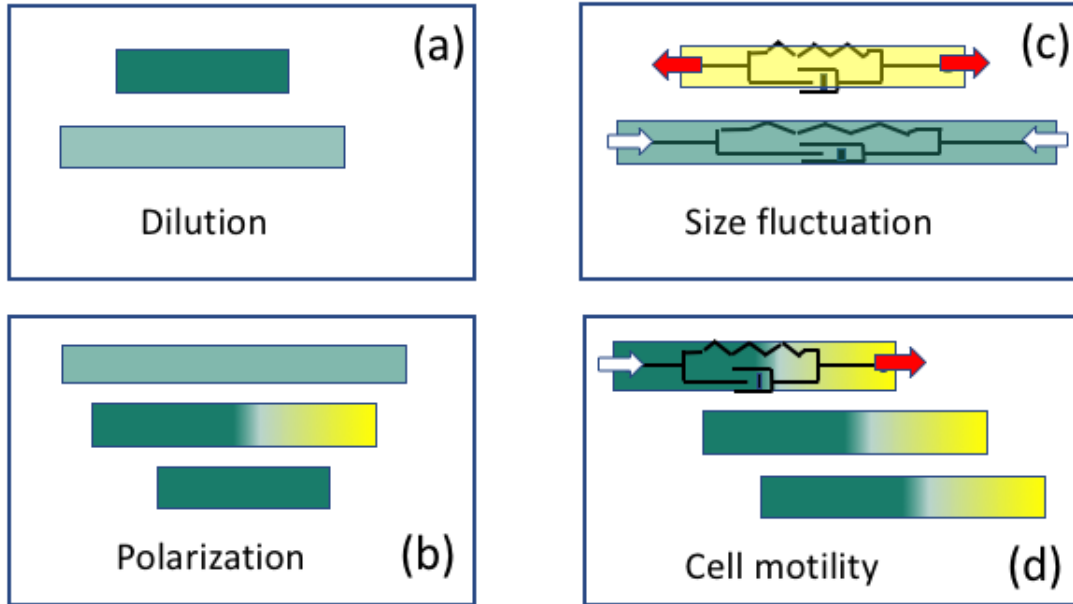


Fig. 3 A summary of the main results of this paper. We discuss how changes in cell size can result in dilution of internal chemical concentration or activity (a). We show that size fluctuations can lead to loss (or gain) of chemical polarization by wave-pinning, as in (Mori et al. 2008) (b). We then introduce mechanical force of protrusion (Rac) or contraction (Rho). In the uniform Rac case (c), cell size fluctuations can occur by virtue of dilution (and loss of Rac activity) when the cell expands. Finally, we show how the mechanochemical model linking GTPase activity to cell protrusion can lead to cell motility.

and similarly for the dependence $A_\rho(G_R)$ of Rho activation rate on the activity of Rac (Holmes and Edelstein-Keshet 2016).

3 Model adaptation (1): Dynamic cell size

The geometry for the single-cell model in Fig. 2 represents a transect across the diameter of the cell.

We keep track of the coordinates for the front and rear cell edges $x_1(t), x_2(t)$, where (WLOG) $x_1(t) < x_2(t)$, so that the cell's length is $L(t) = x_2(t) - x_1(t) > 0$.

Denote by $\Gamma(t)$ the cell interior, i.e. the interval $x_1 \leq x \leq x_2$. A novel feature here is that reaction and diffusion of GTPases is considered on this domain, whose size can change over time.

The motion of cell edges (and the domain $\Gamma(t)$) depend on the regulatory proteins inside the cell. We consider several cases:

1. A cell with one GTPase which causes edge protrusion (e.g. Rac).
2. A cell with one GTPase which leads to edge contraction (e.g. Rho).
3. A cell with both Rac and Rho, with mutual inhibition.

The fact that the domain $\Gamma(t)$ can change with time requires that we modify the RD equations (1). We address this in the next section.

3.1 Changing domain size affects the reaction-diffusion PDEs

In principle, when cell edges protrude or retract, the size of the membrane and cytosol compartments change. Cell volume is known to fluctuate in experimental settings, e.g. when water enters or leaves the cell through aquaporin channels (Zehnder et al. 2015). Here we consider the simplest assumption, that membrane and cytosol compartment sizes both vary proportionately as the cell deforms in 1D. This assumption holds exactly when cells confined to narrow channels elongate while maintaining constant thickness. In more general settings, the approximation is not exact. The opposite extreme case, that cell volume is constant (simply redistributed in another dimension) whereas membrane size expands/contracts is discussed in Appendix D.

We first adopt notation to track material points in the cell. Let Γ_0 denote the reference domain at time $t = 0$. Coordinates in the deformed domain are in lowercase, i.e., x , and coordinates in the original domain are in capitals i.e. X . For convenience, we express location and size in terms of the cell's centroid and radius:

$$x_c(t) = \frac{x_1(t) + x_2(t)}{2}, \quad R(t) = \frac{x_2(t) - x_1(t)}{2}.$$

The mapping between a material point x in the deformed domain, $\Gamma(t)$, and the original site X in the cell at time $t = 0$ is

$$x = A(X, t) = x_c(t) + (X - X_c) \frac{R(t)}{R(0)}.$$

This simplification assumes that the deformation is uniform throughout the cell (i.e. each small volume element of the domain grows/shrinks at the same rate). The speed of the material point x is

$$\begin{aligned} \mathbf{v}(x, t) &= \frac{\partial x}{\partial t} = x'_c(t) + (X - X_c) \frac{R'(t)}{R(0)} \\ &= x'_c(t) + (x - x_c(t)) \frac{R'(t)}{R(t)}. \end{aligned}$$

The velocity of flow of material points is thus decomposed into motion of the cell's centroid ($x'_c(t)$) and expansion or contraction of its radius $R'(t)$. (The rate of change of cell length is $L'(t) = 2R'(t)$.)

A generalized mass balance equation is obtained following the development by (Crampin et al. 1999), as shown in our Appendix. The velocity of material points enters into the continuity equation in the deforming domain. After some standard derivation shown (for pedagogical reasons) in the Appendix, we obtain the following reaction-transport-diffusion equation

$$u_t + \nabla \cdot (\mathbf{v}u) = D\Delta u + f(u), \text{ in } [x_1(t), x_2(t)], \quad (2)$$

with boundary conditions on $\partial\Gamma(t)$ given by

$$-D\nabla u + \mathbf{v}u = 0, \text{ on } \partial\Gamma(t).$$

There are two new terms that appear, namely an effective “advection term”: $\mathbf{v} \cdot \nabla u$ which corresponds to elemental volumes moving with the flow due to local growth and a dilution term, $u \nabla \cdot \mathbf{v}$ due to the local volume change.

For example, if only the centroid moves e.g. $x_c(t) = \beta t$, and $R(t) = R_0$. Then $\mathbf{v} = \beta$, so no dilution takes place. Alternately, if only the radius of the cell increases with $x_c(t) = 0$, and $R(t) = R_0 \exp(kt)$, then $\mathbf{v}(x, t) = kx$. In this case we have both advection and diffusion. In particular,

$$\mathbf{v} \cdot \nabla u = kx \nabla u,$$

and

$$u \nabla \cdot \mathbf{v} = uk.$$

Refer to Fig. 4 for an example of this case.

3.2 Mapping to a constant domain for numerical simulations

To create numerical simulations of our 1D model (while avoiding the complexities of a moving boundary problem), it proves helpful to map the moving boundary problem (2) defined on $\Gamma(t)$ to a stationary domain $\bar{x} \in [-1, 1]$. This can be achieved by the change of variables

$$(x, t) \mapsto (\bar{x}, \bar{t}) = \left(\frac{x - x_c(t)}{R(t)}, t \right). \quad (3)$$

In Appendix B, we show that the resulting equation for u is

$$u_{\bar{t}} = \frac{D}{R^2(t)} u_{\bar{x}\bar{x}} + f(u) - u \left(\frac{\dot{R}(t)}{R(t)} \right), \text{ in } [-1, 1]. \quad (4)$$

Interestingly, the change of coordinates eliminates the advection term, while keeping the dilution term. At the same time, the diffusion coefficient becomes time dependent. The advantage of equation (4) is that it is formulated on a fixed domain. This makes its numerical solutions using a method of lines approach straightforward compared to equation (2) (see Appendix B).

The single GTPase model, so transformed to the domain $[-1, 1]$, then becomes

$$\text{Active:} \quad G_{\bar{t}} = \frac{D}{R^2(t)} G_{\bar{x}\bar{x}} + A(G)G_i - IG - \mathcal{D}(t)G, \text{ in } [-1, 1], \quad (5a)$$

$$\text{Inactive:} \quad (G_i)_{\bar{t}} = \frac{D_i}{R^2(t)} (G_i)_{\bar{x}\bar{x}} - A(G)G_i + IG - \mathcal{D}(t)G_i, \text{ in } [-1, 1], \quad (5b)$$

where

$$\mathcal{D}(t) = \left(\frac{\dot{R}(t)}{R(t)} \right) = \left(\frac{\dot{L}(t)}{L(t)} \right)$$

is an effective “dilution term”, and where $A(G)$ is the activation rate, as before. In the case that cell volume is simply redistributed, while only the membrane component expands or contracts, the term containing $\mathcal{D}(t)$ would be omitted from the second equation (see also Appendix D). The dilution term can be expressed alternately in the above radius or length-dependent forms, used interchangeably in what follows.

3.3 Special case: spatially uniform GTPase

In the case that GTPase activity is spatially uniform inside a cell, we can reduce model (5) to a set of ODEs

$$\begin{aligned}\frac{dG}{dt} &= \left(\beta + \gamma \frac{G^n}{1 + G^n} \right) G_i - IG - G \left(\frac{\dot{L}(t)}{L(t)} \right), \\ \frac{dG_i}{dt} &= IG - \left(\beta + \gamma \frac{G^n}{1 + G^n} \right) G_i - G_i \left(\frac{\dot{L}(t)}{L(t)} \right).\end{aligned}$$

Using mass conservation we reduce this set of two equations to one equation by eliminating the inactive GTPase variable:

$$G_i = \frac{G_T}{L(t)} - G, \quad (6)$$

where G_T is the total GTPase. This leads to

$$\frac{dG}{dt} = \left(\beta + \gamma \frac{G^n}{1 + G^n} \right) \left(\frac{G_T}{L(t)} - G \right) - IG - G \left(\frac{\dot{L}(t)}{L(t)} \right). \quad (7)$$

We later show that this case has interesting consequences when coupled with mechanics. A model of this type, but without the dilution effect was also studied in (Holmes and Edelstein-Keshet 2016).

4 Results (1): Chemistry only (no mechanics)

We first consider results when domain size affects the signaling, but without the effect of signaling on the motion of the cell edges. We show how the classic wave-pining is modified in such cases.

4.1 Parameter values

Since some of our results require numerical simulations, we need biological parameters for the GTPase signaling equations. Typical parameter for the GTPase dynamics are shown in Table 1.

Parameter	Symbol	Value Range	Reference
Basal activation rate	β [s ⁻¹]	0.02 – 0.1	Jilkinine and Edelstein-Keshet; Holmes and Edelstein-Keshet
Auto-activation rate	γ [s ⁻¹]	1 – 25	Jilkinine and Edelstein-Keshet; Holmes and Edelstein-Keshet
Decay-rate	I [s ⁻¹]	1	Jilkinine and Edelstein-Keshet
EC ₅₀ parameter	G_0 [μM]	1	Michaelson et al.; Mori et al.; Jilkinine and Edelstein-Keshet
Active GTPase diffusion	D [μm ² · s ⁻¹]	0.1	Jilkinine and Edelstein-Keshet
Inactive GTPase diffusion	D_i [μm ² · s ⁻¹]	100	Jilkinine and Edelstein-Keshet
Total GTPase	G_T [μM]	1 – 100	
Hill coefficient	n	3 – 25	Holmes and Edelstein-Keshet

Table 1 Parameters for the GTPase intracellular signaling models. Note that G_0 is the GTPase level for half-max GTPase autoactivation in the Hill function of equation (7), prior to non-dimensionalization. A range of up to 1000-fold has been assumed for the diffusion of GTPase protein in the membrane (active) and cytosol (inactive). The upper bound for the Hill coefficient is chosen such that there is a sufficiently large regime in which oscillations are possible.

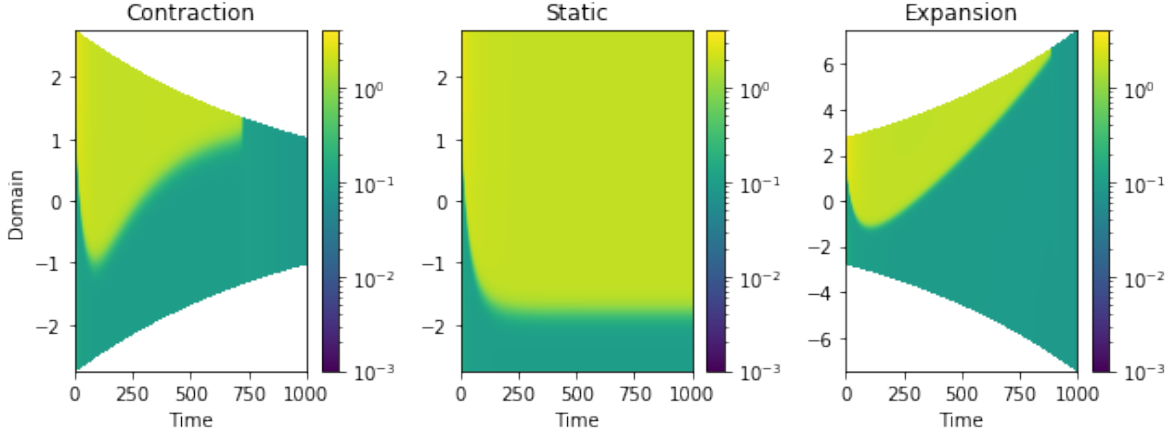


Fig. 4 Effect of domain size on polarization. The GTPase model with changing length (simulated using the mapping to $[-1, 1]$ given by (5)). Initial length is $L = 55\mu\text{m}$ and parameters values: $n = 4, D_i = 1, D = 0.01, \gamma = 2, b = 0.1, I = 1, G_T = 2.5$. Left: A shrinking domain with $R(t) = R_0 \exp(-kt)$, as the cell shrinks G_T increases. Middle: A static domain with $R(t) = R_0$. Right: A growing domain with $R(t) = R_0 \exp(kt)$, (with $k = 10^{-3}$): as the cell grows, G_T decreases. In both cases in which the domain size changes, G_T eventually leaves the parameter regime in which wave pinning is possible. The transition is very rapid.

4.2 GTPase dynamics in constant and fluctuating cell size

In previous work (Holmes and Edelstein-Keshet 2016), predictions of Eqs. (1) was characterized in a static 1D domain using several approximation methods, including Local Perturbation Analysis (LPA). Coexistence of several types of steady state solutions were found. Here, we extend the results to domains with fluctuating size.

We first simulated the GTPase PDE model (5) on a domain whose length is a specified (exponential) function of time. Initial parameter values allow for wave-pinning in each case. Results are shown in panels of Fig. 4 with yellow tint for the high GTPase activity.

In both shrinking and growing model cells, the polarization collapses around $T = 800$. Note the rapidity of the transition from polarized to uniform activity. Loss of polarization if the cell becomes too small is consistent with bifurcation results of (Mori et al. 2011). Loss of polarization when the cell grows too much corresponds to the case where mean total GTPase concentration in the cell drops, also consistent with (Mori et al. 2011). In short, either increase or decrease of cell size eventually moves the system out of the regime of parameters in which wave-pinning can be sustained.

Up to this point, we considered only the GTPase distributions inside the cell, and the effect of changes in cell size on that internal level. To describe the feedback between chemistry and mechanics, we next endow the cell with additional properties that link its size to mechanical forces. The basic ideas follow those of (Zmurchok et al. 2018), but with the adjusted mass balance in place.

5 Model adaptation (2): Cell mechanics

We now specify assumptions and equations for the endpoints of the cell, which then determine its size. As shown in Fig. 2, the cell is modeled as a 1D contractile element of length L and rest length L_0 , analogous to a Kelvin-Voigt element with constitutive relation for the stress, σ given by

$$\sigma(t) = E\epsilon(t) + \eta \frac{d\epsilon}{dt},$$

where E is the cell's Young modulus, η the viscous component and ϵ the strain. Cell motion is in an overdamped regime where inertial terms in the Newtonian force balance are negligibly small. In this regime, the equation of motion becomes $F = \mu v$, where μ is the cell's frictional coefficient. We denote the forces applied at nodes x_1, x_2 by F_1, F_2 respectively. The cell's strain is given by

$$\epsilon = L - L_0 = x_2 - x_1 - L_0.$$

Parameter	Symbol	Value Range	Reference
End point friction	μ [pN · s · μm^{-1}]	$10^3 - 10^5$	Drasdo and Höhme
Cell viscosity	η [pN · s · μm^{-1}]	6×10^1	Palsson
Cell Young's modulus	E [pN · μm^{-1}]	5×10^3	Drasdo and Höhme; Palsson
Cell rest length	L_0 [μm]	$10 - 60$	
Maximum cell force	F_{\max} [pN]	$10^3 - 10^5$	
Cell force half-rate constant	G_c [μM]	$1.25G_0$	
Cell force Hill coefficient	m	$4 - 10$	

Table 2 Mechanical parameters for the model cell. G_0 is defined in Table 1. Parameter values from 3D models are used to inform our 1D model.

5.1 Equations for the cell edges

Given the assumed cell mechanics, the front and rear edge coordinates, x_1, x_2 , satisfy the following equations of motion

$$\mu \frac{dx_1}{dt} = F_1 + E(x_2 - x_1 - L_0) + \eta \left(\frac{dx_2}{dt} - \frac{dx_1}{dt} \right), \quad (8a)$$

$$\mu \frac{dx_2}{dt} = F_2 - E(x_2 - x_1 - L_0) - \eta \left(\frac{dx_2}{dt} - \frac{dx_1}{dt} \right). \quad (8b)$$

Solving the above equation for the time derivatives, we obtain two differential equations for the cell's endpoints

$$\begin{pmatrix} \dot{x}_1 \\ \dot{x}_2 \end{pmatrix} = \frac{1}{\mu(\mu + 2\eta)} \begin{pmatrix} \mu(F_1 + E\epsilon) + \eta(F_1 + F_2) \\ \mu(F_2 - E\epsilon) + \eta(F_1 + F_2) \end{pmatrix}. \quad (9)$$

5.2 Equivalent system for centroid and radius

We can also write this system in terms of the cell's centroid, $x_c(t) = (x_1 + x_2)/2$, and cell's radius, $R(t) = L/2 = (x_2 - x_1)/2$,

$$\begin{pmatrix} \dot{x}_c \\ \dot{R} \end{pmatrix} = \frac{1}{2\mu(\mu + 2\eta)} \begin{pmatrix} (\mu + 2\eta)(F_1 + F_2) \\ \mu(F_2 - F_1 - 2E\epsilon) \end{pmatrix},$$

where $\varepsilon = 2R - L_0$. In simplest form, the latter is written

$$\dot{x}_c = \frac{F_1 + F_2}{2\mu}, \quad \dot{R} = \frac{F_2 - F_1 - 2E(2R - L_0)}{2(\mu + 2\eta)}.$$

From the second equation we recognize the familiar spring-length equation (also directly obtained by subtracting (8)(b-a)):

$$(\mu + 2\eta) \frac{dL}{dt} = (F_2 - F_1) - 2E(L - L_0). \quad (10)$$

In the Appendix, we also show that imposing external forces is equivalent to changing the rest-length of the spring, as in (Zmurchok et al. 2018; Liu 2019).

5.3 Special cases

From the equations for $x_c(t), R(t)$, it is easy to see that in the case of equal forces on the two cell ends, we get

$$F_1 = F_2 = F \quad \Rightarrow \quad \dot{x}_c = F/\mu, \quad \dot{R} = 0,$$

so the cell moves at speed F/μ without deforming. In the case of equal and opposite forces on the two cell ends

$$F_1 = -F_2 = |F| \quad \Rightarrow \quad \dot{x}_c = 0, \quad \dot{R} = (F - E\varepsilon)/(\mu + 2\eta).$$

Hence, the cell does not move, but its size changes.

6 Model adaptation (3): Coupling mechanics and chemical signaling

We now link signaling inside the cell to cell mechanical properties. In (Zmurchok et al. 2018), this coupling was done for the spatially uniform GTPase case without the dilution terms. We extend that model by considering a fully nonuniform GTPase distribution inside a cell correct mass balance for cell size changes.

6.1 GTPase activity affects cell contraction and expansion

The Rac-induced cell protrusion and Rho-induced cell contraction can be modeled in various ways. Here we will assume that Rac and Rho (by assembling actin or activating actomyosin) create forces at cell endpoints. These forces either push the endpoint outwards (Rac) or pull it inwards (Rho). Forces are taken to be a function of the local GTPase level. In the spatially dependent GTPase cases, each cell endpoint can experience a distinct force.

Denote by $G \in \{G_R, G_\rho\}$ the active form of either GTPase. Then the forces $F_{1,2}$ on the cell's endpoints are taken to be

$$F_k(t) = \pm F_{\max} \frac{G^m(x_k, t)}{G_c^m + G^m(x_k, t)}, \quad (11)$$

where $k = 1, 2$. The sign of the force would correspond to an outwards force for Rac and an inwards force for Rho.

According to (11), force builds up continuously as $G(x_k)$ approaches a characteristic level, G_c . The force saturates to a maximal level F_{\max} and the sharpness of the response increases with m . (Note that our framework here appears to be different from (Zmurchok et al. 2018; Liu 2019), where GTPase activity affected the cell rest-length; we show the mathematical equivalence of these two model variants in the Appendix.)

6.2 Complete model equations

In summary, the full model consists of two PDEs for the active and inactive GTPase distributions (with Neumann boundary conditions), equations for the cell centroid and radius, and a GTPase-dependent set of forces on the (transformed) cell ends. That is, the system is as follows:

$$\text{Active GTPase: } G_{\bar{t}} = \frac{D}{R^2(t)} G_{\bar{x}\bar{x}} + f(G, G_i) - G \left(\frac{\dot{R}(t)}{R(t)} \right), \text{ in } [-1, 1], \quad (12a)$$

$$\text{Inactive GTPase: } (G_i)_{\bar{t}} = \frac{D_i}{R^2(t)} G_{i\bar{x}\bar{x}} - f(G, G_i) - G_i \left(\frac{\dot{R}(t)}{R(t)} \right), \text{ in } [-1, 1], \quad (12b)$$

$$\text{Kinetics, BCs: } f(G, G_i) = \left(\beta + \gamma \frac{G^n}{1 + G^n} \right) G_i - IG, \quad G_{\bar{x}} = G_{i\bar{x}} = 0 \text{ for } \bar{x} = \pm 1, \quad (12c)$$

$$\text{Cell centroid, radius: } \dot{x}_c = \frac{F_1 + F_2}{2\mu}, \quad \dot{R} = \frac{F_2 - F_1 - 2E(2R - L_0)}{2(\mu + 2\eta)}, \quad (12d)$$

$$\text{Forces on cell ends: } F_1 = \pm F_{\max} \frac{G^m(-1)}{G_c^m + G^m(-1)}, \quad F_2 = \pm F_{\max} \frac{G^m(1)}{G_c^m + G^m(1)}. \quad (12e)$$

In the following sections, we study variants of this model with and without the diffusion terms, and with the protrusive (Rac, G_R) and contractile (Rho, G_ρ) GTPases acting on their own and together.

7 Results (2): Spatially uniform GTPase linked to forces and dynamic cell size

In this case, we drop the diffusion terms in the first two PDEs in Eqs. (12), so that active GTPase G is time dependent only, uniform throughout the cell. The conservation statement for GTPase reduces to

$$\int_0^{L(t)} (G(t) + G_i(t)) dx = L(t)[G(t) + G_i(t)] = G_T > 0$$

where G_T is the constant total amount of GTPase in the cell. Since $G, G_i > 0$ we can state that

$$G(t) < \frac{G_T}{L(t)}.$$

This implies that the region of interest in the $L - G$ plane is bounded above by the curve $G = G_T/L$. Indeed we show below (Result 1) that this forms an invariant region, i.e. that trajectories do not cross this curve.

Furthermore, since G is spatially uniform, and hence the same at both cell ends, we have that forces on the ends are equal in magnitude but opposite in sign i.e. $F_2 = -F_1$, and the cell tension, $F_T(G) = F_2(G) - F_1(G)$, satisfies $|F_T| = 2|F_1|$. This also means that the cell's centroid remains fixed i.e. $\dot{x}_c = 0$.

Coupling the length of the cell to the GTPase dynamics, Eqn. (7), leads to the reduced model variant to study:

$$\frac{dL}{dt} = \frac{-2E(L - L_0) + F_T(G)}{\mu + 2\eta}, \quad (13a)$$

$$F_T(G) = \pm 2F_{\max} \frac{G^m}{G_c^m + G^m}, \quad (13b)$$

$$\frac{dG}{dt} = \left(b + \gamma \frac{G^n}{1 + G^n} \right) \left(\frac{G_T}{L} - G \right) - IG - G \left(\frac{\dot{L}}{L} \right). \quad (13c)$$

The sign on the force terms in (13b) is $+$ for a protrusive GTPase ($G = G_R$) and $-$ in the contractile GTPase case ($G = G_\rho$). We have reduced the original system (12) to the two coupled ODES (13a) and (13b) for $L(t), G(t)$. This system can be studied in the $L - G$ phase plane. Below we explore the detailed behavior of this system.

To ensure that the cell length remains positive in the contractile (Rho) case we require that $EL_0/F_{\max} > 1$. In addition, we assume that in this section the force switches “ON” at $G_c > 1$; the case in which $G_c < 1$ follows readily.

Result 1 (Invariant Region) *The region defined by*

$$\Delta := \{(L, G) : L > 0; G \geq 0; G \leq G_T/L\}$$

is invariant with respect to the flow given by equations (13).

Proof Since $EL_0/F_{\max} > 1$, we have that $L' > 0$ for $L > 0$, and similarly $G' > 0$ whenever $G = 0$. So flow cannot leave the region through the axes. Now consider the direction of the flow along the boundary curve $f(L) = G_T/L$. The normal vector along the curve is given by $(1, L^2/G_T)$, then computing the component of flow along this normal direction, we find

$$(L'(t), G'(t)) \cdot (1, L^2/G_T) < 0.$$

so the flow is *into* the region, and cannot leave through this boundary. Hence flow is trapped in the region Δ , which is thus invariant.

In Fig. 5, we show typical phase plane behavior of the system (13) for the contractile Rho ($G = G_\rho$, left) and protrusive Rac ($G = G_R$, right) cases. In both cases we find the region Δ bounded by the (thick black) curve $G = G_T/L$. The level of total GTPase, G_T controls the position of this curve, so that the region is larger for larger values of G_T . The nullclines, obtained by setting $dL/dt = 0$ in (13a) and $dG/dt = 0, \dot{L} = 0$ in (13c) have shapes with the following features: the L nullcline (black) is sigmoidal, but its orientation flips between the two cases. The G nullcline (grey) is “Z-shaped”. It remains to determine how many possible steady states can occur at intersections of such curves, and which parameters govern possible bifurcations.

7.1 Sharp-switch analysis

To help explore this question, we use a common shortcut, the sharp-switch approximation (Holmes and Edelstein-Keshet 2016) in the L equation. Next we estimate the number of possible steady states.

Result 2 (Number of steady states) *Consider ODE (13c) with $L(t)$ set to either of the two steady states of the ODE (13a). Then ODE (13c) has either one or three positive steady states.*

Proof In the contractile (Rho) case, the L nullcline is given by:

$$L_{eq} = L_0 - \frac{F_{\max}}{E} \frac{G^m}{G_c^m + G^m}.$$

In the protrusive (Rac) case, the minus sign is replaced by $+$.

We assume that the switch is sharp and approximate L by $L_\infty \in \{L_0, L_0 - F_{\max}/E\}$. The nullcline for G can be written as:

$$L[A(G) + I] + \dot{L} = A(G) \frac{G_T}{G}, \quad L, G > 0,$$

where $A = (b + \gamma h(G))$ and $h(G)$ is the Hill-function in (13a). Substituting the expression for \dot{L} from the ODE (13c), leads to a more complicated nullcline equation which we do not display, but which leads to the

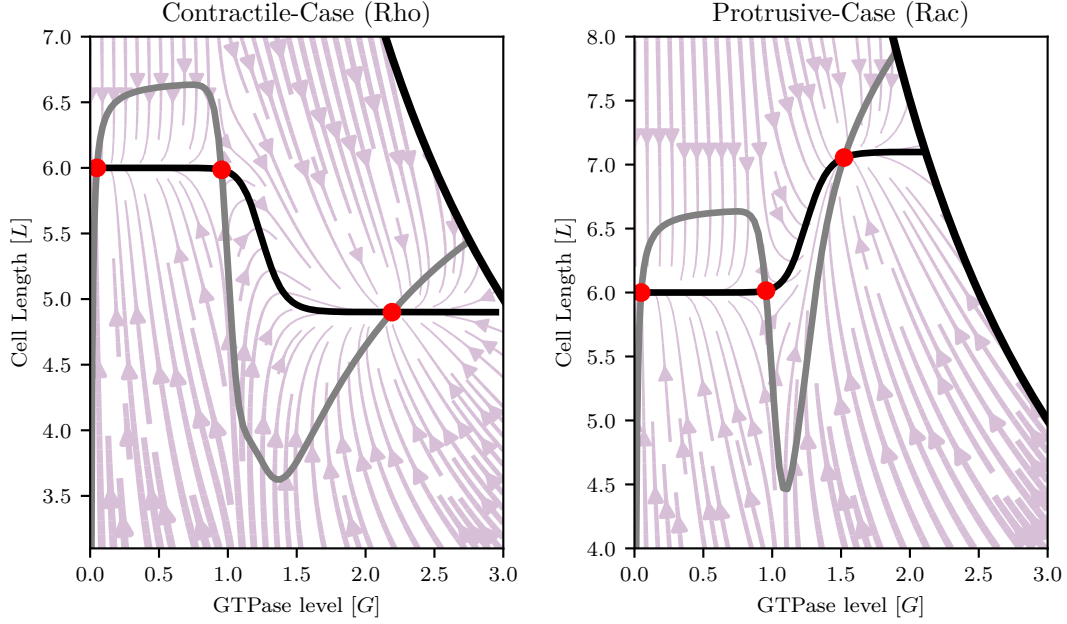


Fig. 5 Phase-plane plots for the contractile (left: Rho) and protrusive (right: Rac) cases of the dynamical system (13). In solid black L nullcline, and in grey the G nullcline. The steady states are shown by red dots. Note the invariant region, bounded by the curve $L = G_T/G$. Here $G_T = 15$, $G_c = 1.25$, $\gamma = 2.5$, $n = 25$, $m = 16$, $L_0 = 6$, and other parameter values are as in Table 1, and Table 2. In both cases, the most left (G_1) and most right (G_3) steady states can be approximated using a sharp switch approximation, the middle steady states are saddles.

sigmoidal curve plotted in Fig. 5 (black) and in Fig. 6 (blue). Observe that the direction of this switch flips between the Rac and the Rho cases, as shown in the top and bottom panels of Fig. 6, respectively.

As we are seeking steady states, we may set $\dot{L} = 0$, simplifying the resulting equation to

$$L = \frac{G_T (b + \gamma h(G))}{G (I + b + \gamma h(G))} \equiv n(G),$$

where we have defined $n(G)$ as the rational function that appears. We note that asymptotically $n(G)$ behaves as:

$$\lim_{G \rightarrow 0} n(G) = \infty, \quad \lim_{G \rightarrow \infty} n(G) = 0.$$

To find intersections of $n(G)$ with L_∞ we must solve:

$$G^{n+1} L_\infty (I + b + \gamma) - G^n G_T (b + \gamma) + G L_\infty (I + b) - b G_T = 0.$$

Let p be the number of positive solutions of this polynomial. Since the sequence of the polynomial's coefficients features three sign changes, we have by Descartes' rule that $3 - p$ must be non-negative and even (for a statement of Descartes' rule we refer the reader to Appendix 2 of (Murray 1989)). We conclude that $p = 1$ or 3.

Result 2 implies that in most cases we have either one or three solutions. Note that in the most general case when L is not set equal to either of its two steady-states, Descartes' implies that there may be 1, 2, 5 or 7 steady states. However, since Result 2 restricts the number of steady states when $L = L_\infty$ these additional

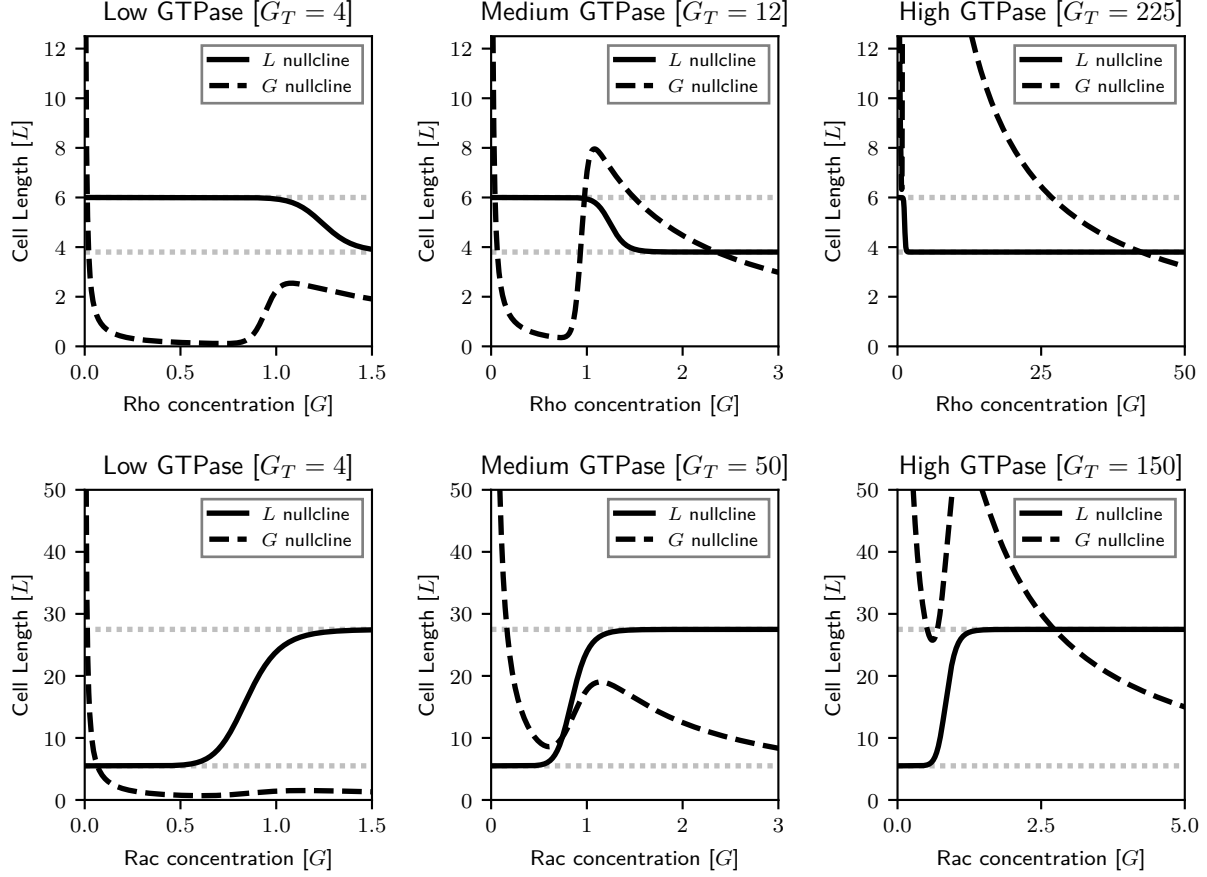


Fig. 6 Possible nullcline configurations. Top: contractile GTPase (Rho) case; Bottom: protrusive GTPase (Rac) case. Top: For Rho, the left panel shows the existence of G_1 . The middle panel shows the bistable case, i.e. two steady states in which the cell is large and GTPase is small (G_1 , and G_3). The right panel shows the existence of a single steady state G_3 . Other parameters $\gamma = 2.5, b = 0.02, I = 1, L_0 = 6$. The dotted lines are the upper and lower sharp switch approximations of the sigmoidal L nullcline. Bottom: For Rac, the middle panel demonstrates the case where a stable limit cycle oscillation is expected, a situation that cannot occur in the Rho case. Other parameters $\gamma = 0.9, b = 0.1, I = 1, L_0 = 6$. For the values of the approximate steady states G_1, G_2 , and G_3 see Appendix C.1.

steady states must occur in the thin region $G \sim G_c$ in which L transitions between the two possible value for L_∞ . Thus in the vast majority of cases we only have 1 or 3 steady states. See also Fig. 6.

The sharp-switch approximation leads to explicit values for some of the steady states of the system, their eigenvalues, and hence full characterization of their stability and conditions for existence. The detailed calculations are provided in Appendix C. A brief summary is given in Table 3. This approximation does not allow easy computation of steady states that occur when nullclines intersect along the upswing portion of the switch. However, the geometry of such intersections allows us to determine stability nonetheless, using geometric methods described in (Murray 1989) (see also Appendix C for linear stability analysis).

In the contractile GTPase (Rho) case, we find three steady states, all stable nodes, with possible coexistence of all three (These are separated by steady states that occur on the portion of the switch not captured by the approximation). In the protrusive (Rac) case there are either two coexisting stable steady

GTPase Level	L_{eq}	G_{eq}	Stability
$G < \min(1, G_c)$	L_0	$\frac{bG_T}{L_0(b+I)}$	stable node
transition	?	?	Rho: saddle. Rac: unstable, saddle
$1 < G < G_c$	L_0	$\frac{(b+\gamma)G_T}{L_0(b+\gamma+I)}$	stable node
transition	?	?	Rho: saddle. Rac: unstable, saddle
$G > \max(G_c, 1)$	L_1	$\frac{(b+\gamma)G_T}{L_0(b+\gamma+I)}$	stable node

Table 3 Sharp switch approximated steady state summary. Here $L_1 = L_0 - (F_{\max}/E)$ for Rho and $L_1 = L_0 + (F_{\max}/E)$ for Rac. The transitions in the table can contain one or more steady states. In case of a single steady state at the transition, that state is unstable. Note that the number of coexisting steady states depends on the parameters. See text and Appendix C for details.

states (separated by a steady state not captured by the approximate) or no coexisting stable steady states at all. When no stable steady states exist we must have a stable limit cycle, since Δ is invariant.

7.2 Simulations

We simulated the model for the spatially uniform Rho, and Rac case (see Fig. 7), starting with a cell at its rest-length. Results are shown in the form of a kymograph, with time on the horizontal axis, and a profile of the cell and its internal active GTPase concentration on the vertical axis.

In both the Rho and Rac case of the single-GTPase model, when the total amount of the GTPase, G_T in the domain is too low (left panels), there is no response. For high G_T (right panels), the system is triggered to switch to the high GTPase steady state (shaded yellow). For Rho (top panels in Fig. 7), the cell contracts as a result, and the high activity state becomes amplified even more due to the smaller volume in which it is concentrated. In contrast, in the Rac case (Bottom panels of Fig. 7), expansion caused by high Rac results in a larger cell, but also dilutes Rac activity, depressing it to a lower level.

In the Rac, but not the Rho case, the conflicting effects of expansion and dilution can set up an oscillatory behavior (bottom middle panel, Fig. 7). The cell alternates between long and short phases, with fluctuations in its Rac activity.

7.3 Bifurcation diagrams

Finally, we characterized the regimes of behavior in the spatially uniform cases by creating bifurcation plots of model (13). Results are shown in panels of Fig. 8 for Rho (top) and Rac (bottom). It is evident that a region of tristability can exist in the Rho case (labeled C), whereas the Rac case has a regime in which limit cycle oscillations can exist. Panels on the left should be compared with the 2-parameter bifurcation plot for the single-GTPase case (Fig. 3a) in (Holmes and Edelstein-Keshet 2016). The distinction here is that we have taken cell size into account, which increases the number of possible steady states and introduces the possibility of Hopf bifurcations.

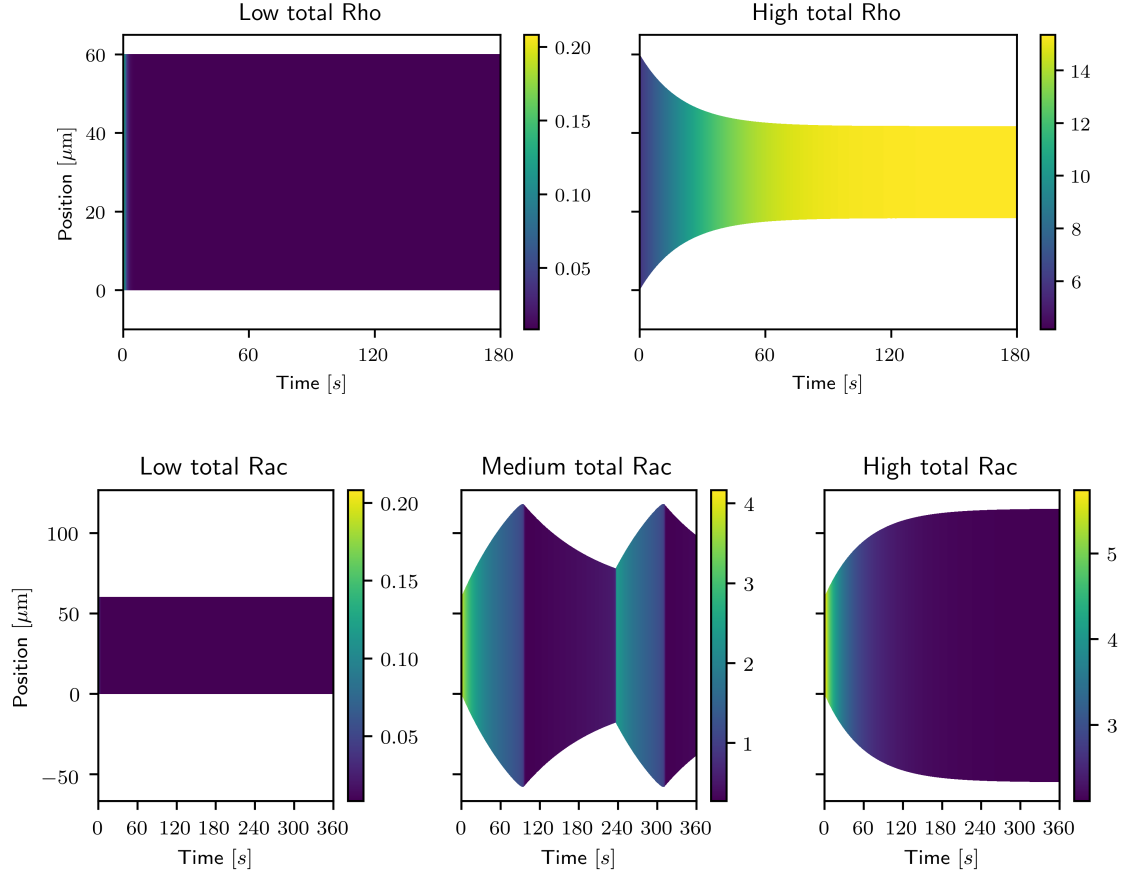


Fig. 7 Simulation of a cell with uniform internal GTPase. Top: Rho, the GTPase that leads to contraction. Bottom: Rac, the GTPase that leads to cell protrusions. Left panels: Low total amount of GTPase, $G_T = 2.5$: no change takes place in either case. Right panels: High total GTPase, $G_T = 50$: the cell becomes uniformly high in Rho/Rac and hence shrinks/expands, respectively. Bottom Middle: Cell with intermediate total Rac and parameters such that oscillation is possible. Same parameters as the bottom middle of Fig. 6 ($E = 250 \text{ [pN} \cdot \mu\text{m}^{-1}]$). Initially, the cell is at its “rest-length” $L(0) = L_0$, and GTPase is uniformly set to G_T/L . In the Rac case the cell’s stiffness is $E = 500 \text{ [pN} \cdot \mu\text{m}^{-1}]$, while in the Rho case it is $E = 1500 \text{ [pN} \cdot \mu\text{m}^{-1}]$. This choice ensures that the cell does not vanish i.e. $EL_0/F_{\max} > 1$.

7.4 Extensions to a Rac-Rho model

So far, we explored only the single GTPase model, for either Rac or Rho acting alone. We asked how conclusions would change if both Rac and Rho operate simultaneously (with mutual inhibition) as in (Holmes and Edelstein-Keshet 2016; Zmurchok et al. 2018; Zmurchok and Holmes 2019). We briefly examined the spatially uniform case using the same sharp switch approximation. Rac and Rho each have two applicable thresholds: one for turning on the self-activation, and another for the cell length, which implies three possible cases for equilibrium levels. With two GTPases in the model, there would be nine possible equilibria, (which may not all coexist in the same parameter regime). There are many parameters to consider. From preliminary exploration, we are able to find multi-stability and oscillatory regimes consistent with results for the single GTPase model. We did not find new behaviors unique to the two-GTPase model, but see also (Zmurchok and Holmes 2019) for further results.

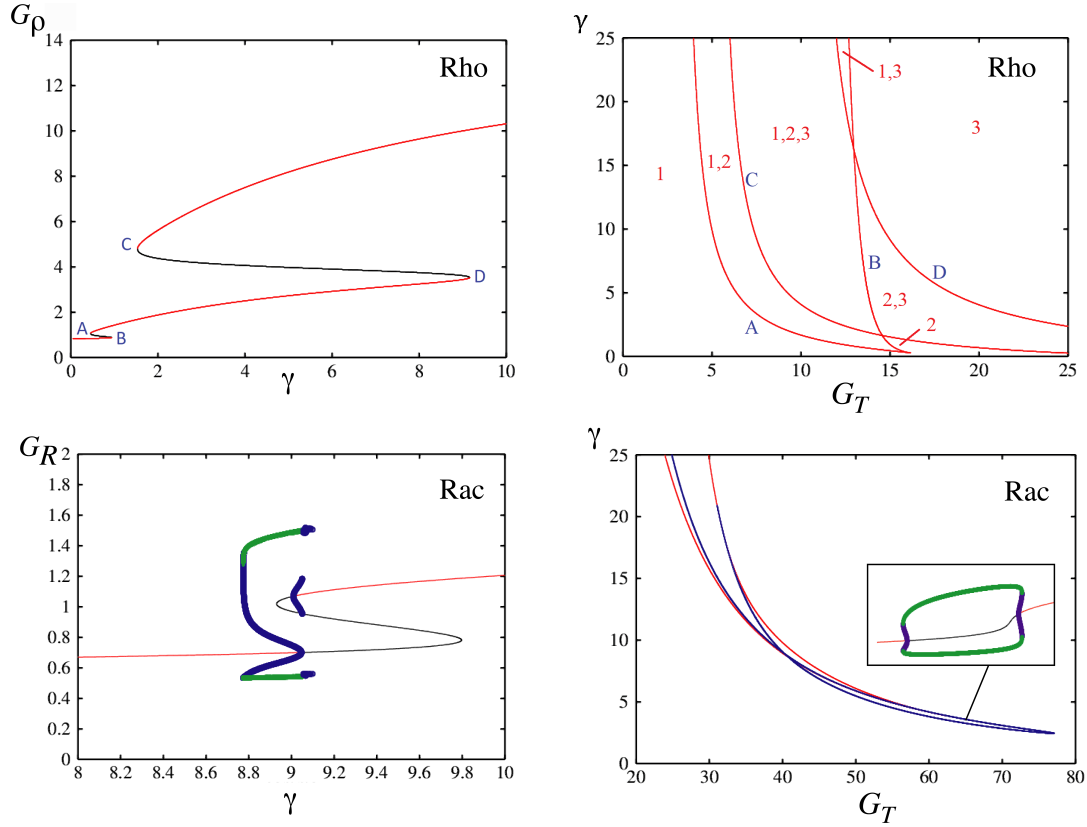


Fig. 8 Bifurcation diagrams for the spatially uniform GTPase cases. Top: the contractile (Rho) case, showing the possibility of tristability. Bottom: The protrusive (Rac) case. Left panels: one-parameter bifurcation with respect to the feedback activation rate, γ . Right panels: two-parameter bifurcation plot with respect to total GTPase, G_T and γ . The fold bifurcations in the Rho case (top left) labeled A, B, C, D, are tracked by curves with the same labels in the two-parameter plot (top right). Numbers 1,2,3 indicate existence of the corresponding steady states in regions of the same plot. (For example, “1,2,3” indicates existence of all three equilibria G_1, G_2, G_3 , as discussed in Appendix C. The parameters are $b = 1, I = 5, m = n = 20, L_0 = 3, \frac{2E}{\mu+2\eta} = 5, \frac{2F_{max}}{\mu+2\eta} = 10, G_c = 4, G_T = 15$. Bottom: Left: a supercritical Hopf bifurcation is evident at $G_T = 40$. Right: the inset shows a limit cycle that exists in the range of $G_T = 65$ and $3.2 < \gamma < 3.6$. Limit cycles are possible only in the Rac case. The parameters are $b = 1, I = 10, m = n = 8, L_0 = 5.5, \frac{2E}{\mu+2\eta} = 5, \frac{2F_{max}}{\mu+2\eta} = 55, G_c = 0.85$.

8 Results (3): Spatially distributed GTPase dynamics in the full coupled model

Here we numerically solve the full PDE model (12) with dynamic cell size, and forces created at the cell ends by local GTPase. We take into account dilution, and examine both contractile and protrusive GTPase. Details of the numerical implementation is given in Appendix B.

8.1 Single GTPase

Results are shown as kymographs in Fig. 9. Cells were initialized at rest-length, $L(0) = L_0$, with elevated GTPase (step function) at one edge. We tested both stiff (left) and soft (right) cells, by varying the parameter E .

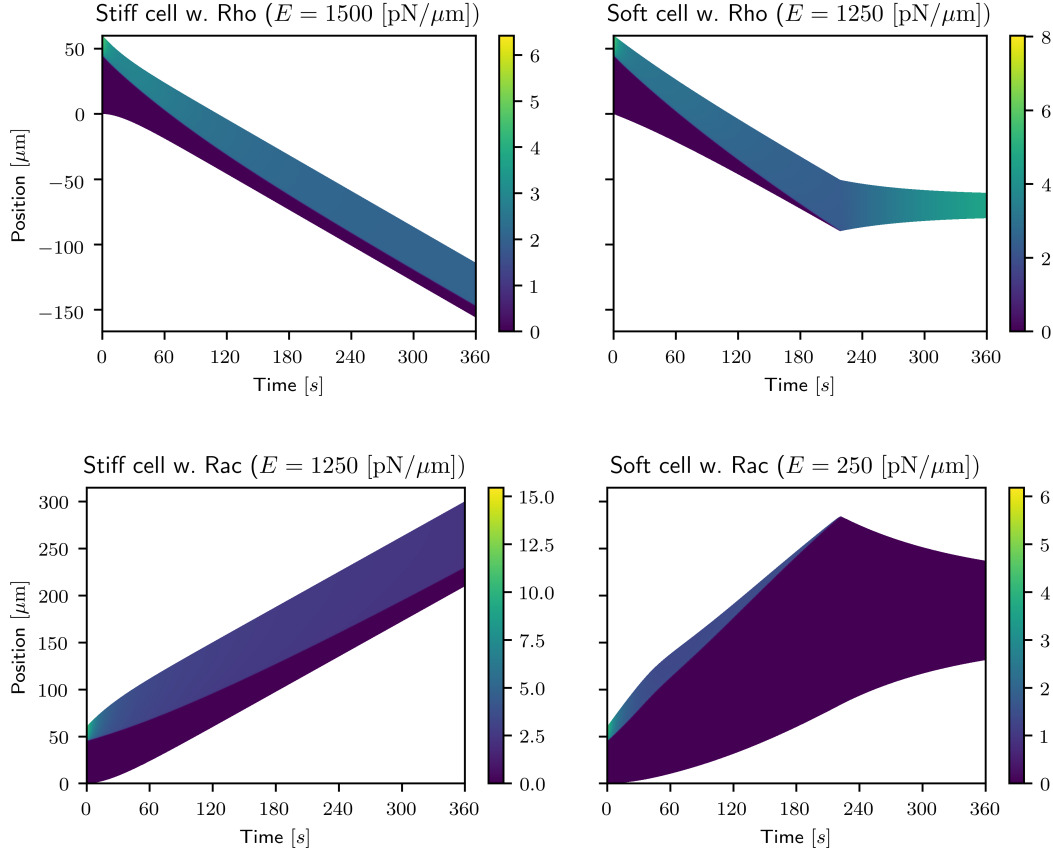


Fig. 9 Full spatiotemporal simulations of a single GTPase in the 1D cell. (Shown is the concentration of active GTPase.) Top: the contractile (Rho) case. Bottom: the protrusive (Rac) case. Initially, cell length is $L(0) = L_0$. Active GTPase initialized with step function at the top edge of the cell. Left: A stiff cell with $G_T = 25$; length hardly changes in either case and polarization is maintained. Right: A soft cell with $G_T = 10$, showing significant length change. Once the cell shrinks or expands too much, it loses polarization.

For the Rho case (top row of Fig. 9), motility is by “pushing” or “squeezing” from the rear. That is, as the edge of the cell with high Rho activity contracts inwards, the cell’s elastic “spring” pushes the other edge outwards. If the cell is stiff, both edges then translocate in a nearly linear fashion. A soft cell never manages to compensate for the contraction of the rear edge. Eventually, the cell becomes too small to support a polarized GTPase pattern. Then polarization is lost and the whole cell contracts and keeps shrinking, amplifying the Rho concentration.

The Rac GTPase case is shown in the bottom row of Fig. 9. The cell moves in the direction of the Rac gradient (edge protrudes outwards). As before, for stiff cells (left), the rear keeps up with the front due to the restoring spring-force; a tight GTPase gradient is formed and persists in the moving cell. In the soft cell (right), the rear edge is only weakly pulled along by the elastic restoring force. Once the cell is “too long”, polarization is lost, Rac activity collapses abruptly to a low uniform level, and the cell shrinks.

From the simulation results (and many replicates, not shown) we draw the following overall conclusions. (1) The direction of motion depends on initial conditions and GTPase type. Cells move towards the direction of Rac and away from the direction of Rho gradient in the single GTPase simulations. (2) Results demonstrate polarization (gain or loss) as well as size changes and the interplay between these. (3) Polarized cells

can become non-polar by growing or shrinking too much - both extremes drive the system away from the polarization parameter regime. (4) Softer cells are particularly prone to depolarization as restoring cell size takes longer than the timescale of loss of polarization: see the bottom row of Fig. 9. (Equivalently, cells with large protrusive or contractile forces F_{\max} are also prone to depolarization.) (5) Cells with two peaks of Rac at opposite ends tend to stretch and lose the ability to polarize. Two peaks of Rho cause cells to shrink too much and lose polarization. (6) Changing the cell's internal viscosity does not strongly affect the above result, but it changes the time scale of cell deformation.

8.2 Mutual antagonism: Rac and Rho in the same cell

Finally, we simulated the Rac-Rho mutually antagonistic full model as described in the “Two GTPase model” of Section 2. The forces of protrusion or retraction on the cell end x_k are assumed to depend on both Rac and Rho as follows:

$$F_k(t) = (-1)^k F_{\max} \left(\frac{R^m(x, t)}{G_c^m + R^m(x, t)} - \frac{\rho^m(x, t)}{G_c^m + \rho^m(x, t)} \right) \Big|_{x=x_k},$$

for $k = 1, 2$. In the full model equations (12), this replaces equations (12e). Note that since Rac and Rho are mutually antagonistic, one will dominate at each of the cell endpoints.

Cells were initialized with the same parameters, spatially uniform GTPase, with superimposed Gaussian noise in inactive Rho. Sample results are shown in Fig. 10.

These results (including others, not shown) can be summarized as follows: (1) The evolving GTPase pattern is determined by the initial conditions. (2) Rac and Rho segregate to mutually exclusive regions in the cell. (3) Polarized motile cells spontaneously gain active Rac at the “front” and Rho at the “rear”. (4) Cells with more than a single transition layer display rich dynamics, in particular as plateaus of active GTPase transition from the interior to a cell edge. This causes some cells to stall, and others to start moving, as shown in Fig. 10. (5) Cells with high Rac at both ends get larger, whereas those with high Rho at both ends shrink. Such metastable states can persist for a long time.

In short, the full model with Rac-Rho mutual inhibition displays a diverse set of behaviors not seen in model variants that neglect the full spatio-temporal GTPase distribution, or that assume static cell size.

9 Discussion

Interplay between the activity of GTPases, the contraction or expansion of a cell, and resultant feedback to GTPase activation was previously explored in a related framework by (Zmurchok et al. 2018). Our approach here differs in two main respects: (1) GTPase is no longer assumed to be spatially uniform, and (2) cell size dynamics is considered in the mass balance of the GTPase.

Accounting for the spatial distribution of the GTPases inside a cell leads to new features that were absent in (Zmurchok et al. 2018). These include (a) delay while the internal GTPase activity reorganizes spatially, (b) the possibility of polarization and net motion, rather than just cell expansion or contraction (c) cases where the cell stalls when plateaus of GTPase form at both cell edges, and (d) loss of polarization if the cell gets too large or too small.

Despite the simplicity of the model, initially comprised of a single GTPase (with active/inactive forms) in 1 spatial dimension, we find a variety of possible behaviours even in the spatially homogeneous case, depending on the action of the GTPase. The simplicity of the model then permits analysis of steady states, stability, and Hopf bifurcations. Analysis is considerably more challenging in the more detailed models.

There are two ways that cell size affects the results of bifurcation analysis. 1) through the definition of length and time scales; and 2) by diluting or concentrating the internal signaling activity, as shown by detailed mass balance, and known classically. This in turn, also affects whether the cell can have a polarized

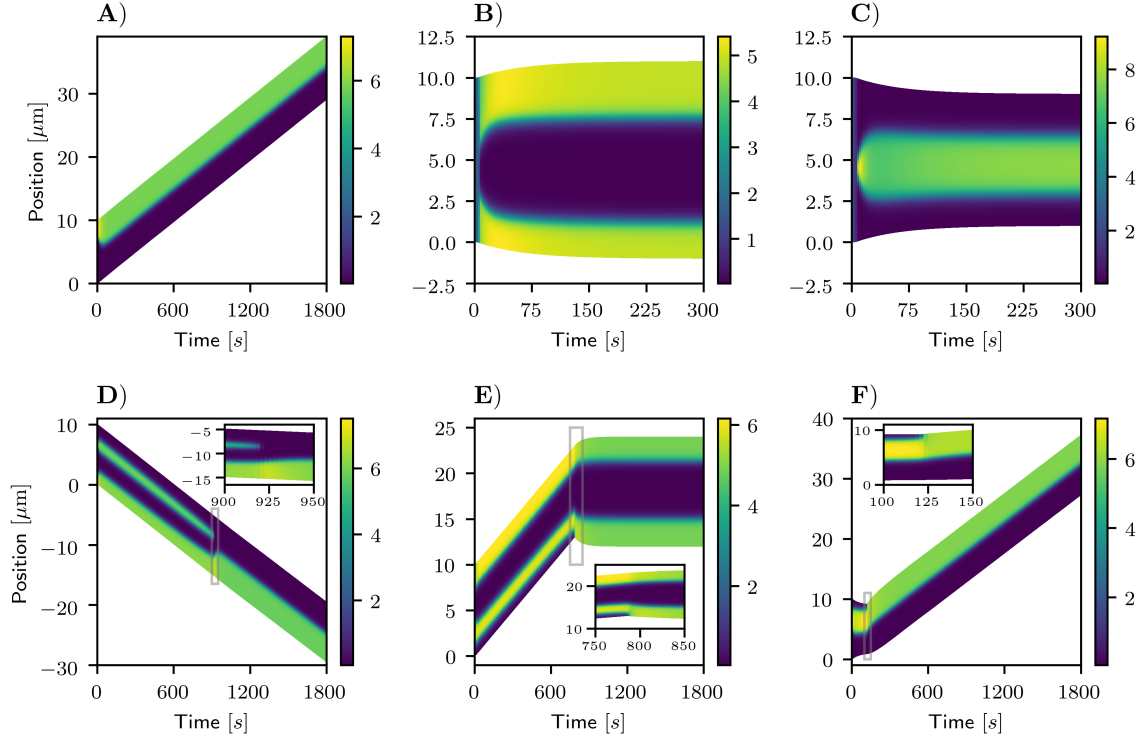


Fig. 10 Various possible behaviours in the full Rac-Rho model with mutual inhibition. Shown is the profile of active Rac. (Active Rho profile is complementary.) Parameters are $L_0 = 10\mu\text{m}$, $m, n = 4$, $\gamma = 5$, $G_T = 4$. Plots differ in initial inactive Rho (small Gaussian noise about the uniform steady state); other GTPase initially uniform across the cell. (A) Polarized cell with Rac front moves at constant rate. (B) Stationary cell with high Rac at both ends expands. (C) Cell with high Rho at both ends contracts without moving. (D) Cell with two peaks of Rac becomes uni-polar (at around 900 s) and continues to move in the same direction. (E) Similar to D, but with reorganized Rac eventually stalling the cell. (F) Initially static cell with an internal region of high Rac, which moves toward a boundary, thus mobilizing the cell. Insets: expanded views of regions of interest shown in grey rectangular portions of the trajectories.

state. The single GTPase model of Eqs. (1) can sustain “polarized” wave-pinning solutions, but if the domain grows (or shrinks) too much these are lost. This is consistent with (Mori et al. 2011) where the bifurcation parameter ϵ depended on cell size.

We showed that the cell could undergo cycles of expansion and contraction in the case of a Rac-like GTPase that pushes out the cell edges. Recent work on cell oscillations (in the context of confined epithelial sheets) is given in (Peyret et al. 2019), and a review of cycles of protrusion and retraction in experimental and theoretical models of the cell edge is found in (Ryan et al. 2012). Cycles also occur in paper by (Dierkes et al. 2014), who consider a similar treatment of dilution (of myosin concentration) when the cell stretches, and a mechanical contractile unit driven by myosin. Unlike our model, their chemical equation is simply linear return to a baseline level c_0 , with a similar dilution term $(c/\ell)(d\ell/dt)$. Their oscillations stem from an assumption that the “spring” governing cell length has a nonlinear (cubic) term $(K(\ell))$.

One can argue that some cells deform and redistribute their protrusions while maintaining a fixed volume. For this reason, we also considered a model variant with fixed volume. Qualitatively, the two variants are similar, though some features differ. See Appendix for a comparison. It is easy to generalize the model (8) to the version in the recent paper by (Bui et al. 2019) who used distinct values of the frictional coefficient μ at the front and the rear of each cell.

While this study demonstrated the behaviour of a simple GTPase system in 1D, it prepares the ground for 2D simulations where cell shape can be explored more fully. It also opens the way to considering how cells interact with one another and how mechanochemical feedback between those cells affects emergent behavior at the scale of a tissue.

While it is straightforward to carry out analysis in the uniform case, such analysis is more challenging in the spatially distributed cases. Since in our model the forces on the cell ends solely depend on the active GTPase concentrations at the cells ends, a worth while question for future research is whether it is possible to replace (in some limit) the full PDE by two ODEs tracking the amount of active GTPase at the cell ends. A distinct challenge is the emergence of more complicated transient dynamics (see Fig. 10), which persist on time-scales significant for cellular behaviour. This highlights the need to not only better understand the asymptotic behaviour of such equations but also their transient dynamics. This becomes even more urgent in view of future models containing more details and multiple cells.

A Mass balance on growing or shrinking domain

Consider a prototypical reaction diffusion equation for some concentration $u(x, t)$ in conservative form,

$$u_t = -\nabla \cdot \mathbf{j}(u) + f(u), \quad \text{in } \Gamma(t),$$

where $\mathbf{j}(u)$ is the particle flux. Further, assume no-flux boundary conditions on the boundary of the domain, $\partial\Gamma(t)$. In integral form, we write a conservation law for a small volume element $V(t) = [x(t), x(t) + \Delta x(t)]$

$$\frac{d}{dt} \int_{V(t)} u(x, t) dx = \int_{V(t)} [-\nabla \cdot \mathbf{j} + f(u)] dx.$$

Using the Reynolds transport theorem the left hand side is equivalent to

$$\frac{d}{dt} \int_{V(t)} u(x, t) dx = \int_{V(t)} [u_t + \nabla \cdot (\mathbf{v}u)] dx,$$

where \mathbf{v} is the velocity of the material point $x(t)$. We then obtain the following reaction-transport-diffusion equation

$$u_t + \nabla \cdot (\mathbf{v}u) = D\Delta u + f(u), \quad \text{in } [x_1(t), x_2(t)]. \quad (14)$$

Similarly, the boundary conditions on $\Gamma(t)$ become

$$-D\nabla u + \mathbf{v}u = 0, \quad \text{on } \partial\Gamma(t).$$

We have two new terms

1. An advection term, $\mathbf{v} \cdot \nabla u$, which corresponds to elemental volumes moving with the flow due to local growth.
2. A dilution term, $u\nabla \cdot \mathbf{v}$, due to local volume changes.

B Numerical Implementation

B.1 Mapping to a constant domain

It is most convenient to discretize and numerically solve the PDEs on a constant domain. Hence a mapping is used to transform the growing/shrinking cell to the interval $[-1, 1]$. This can be achieved by the following change of variables

$$(x, t) \mapsto (\bar{x}, \bar{t}) = \left(\frac{x - x_c(t)}{R(t)}, t \right).$$

Note that \bar{x} is the location in the new domain $[-1, 1]$, whereas x is located in the cell domain $[x_1(t), x_2(t)]$. Carefully applying the chain-rule leads to

$$\begin{aligned} u_{\bar{x}} &= \frac{\partial u}{\partial x} \frac{\partial x}{\partial \bar{x}} = u_x R(t) \\ u_{\bar{t}} &= \frac{\partial u}{\partial t} \frac{\partial t}{\partial \bar{t}} + \frac{\partial u}{\partial x} \frac{\partial x}{\partial \bar{t}} \frac{\partial t}{\partial \bar{t}} = u_t + u_x (\bar{x}R'(t) + x'_c(t)), \end{aligned}$$

where we have used $x = \bar{x}R(t) + x_c(t)$ and $t = \bar{t}$ in the transformation. Substituting these results into Eqn. (2), we obtain

$$u_{\bar{t}} - u_{\bar{x}} \frac{\bar{x}R'(t) + x'_c(t)}{R(t)} + \frac{x'_c(t) + \bar{x}R'(t)}{R(t)} u_{\bar{x}} + u \frac{R'(t)}{R(t)} = \frac{D}{R^2(t)} + f(u), \quad \text{in } [-1, 1].$$

Cancelling two terms on the LHS. and rearranging leads to

$$u_{\bar{t}} = \frac{D}{R^2(t)} u_{\bar{x}\bar{x}} + f(u) - u \left(\frac{\dot{R}(t)}{R(t)} \right), \quad \text{in } [-1, 1].$$

The total amount of GTPase on the interval $[-1, 1]$ becomes time dependent through

$$G_T = \int_{-R(t)}^{R(t)} (G + G_i) dx = R(t) \int_{-1}^1 (G + G_i) dy.$$

B.2 Changing rest length is equivalent to imposing additional force

It is easy to see, from Eqn. (10) that adjusting the cell's rest length, L_0 is equivalent to assuming that additional forces act on the cell:

$$(\mu + 2\eta) \frac{dL}{dt} = (F_2 - F_1) - 2E(L - L_0) = -2E(L - (L_0 + \Delta L_0)), \quad (15)$$

where $\Delta L_0 = (F_2 - F_1)/2E$. In other words a change of ΔL_0 is equivalent to an additional force of $-2E\Delta L_0$.

In (Zmurchok et al. 2018) and (Liu 2019) only the spatially uniform G model variants were considered. There, cell length was modeled by (15), with

$$\Delta L_0(G) = \pm b \frac{G^m}{G_c^m + G^m}.$$

Rac (+) is assumed to increase L_0 and Rho (-) to decrease it, so the sign of the Hill function depends on the given GTPase.

As shown here, the assumptions that GTPases work through modification of the cell's effective rest length is mathematically equivalent to assumptions we make about GTPase-dependent load forces on the cell ends.

B.3 Numerical methods

Each cell introduces a set of mechanical equations for its endpoints i.e. equation (9). Next, each cell contains K GTPases, that is we include K sets of reaction-diffusion equations (1). The cell interior is divided into a cell-centered grid with uniform length $h = 1/N$, where N is the number of grid cells per unit length. Here we use $N = 2^{10}$. The second order derivative is discretized using a second order cell centered finite difference. For more detailed information on the numerical method, see (Gerisch 2001). This results in M total grid points per GTPase species, and K GTPase species. The resulting state vector is given by

$$y = \begin{pmatrix} x_1 \\ x_2 \\ G_{1,1} \\ G_{1,2} \\ \vdots \\ G_{K,M} \end{pmatrix}$$

where $G_{j,k}$ denotes the concentration of the k -th GTPase at the j -th spatial grid point. The temporal evolution of the state of the cell can be written as:

$$\frac{dy}{dt} = f(t, y),$$

where $f(t, y)$ is a function whose first two entries contain equation (9) and the final KM entries are the result of the spatial discretization of the GTPase PDEs.

The resulting system of ordinary differential equations are integrated using the ROWMAP integrator (Weiner et al. 1997), an specialized integrator for large stiff ODEs (such systems are commonly the result of spatially discretizing PDEs). Here we use the ROWMAP implementation provided by the authors of (Weiner et al. 1997)¹. The ROWMAP-integrator (written in Fortran) is wrapped for easy use in a Python environment using `f2py`² (`f2py` provides a connection between the Python and Fortran languages) and integrated into `scipy`'s³ integrator class (a package providing several different techniques to integrate ODEs). The spatial discretization (right hand side of ODE) is implemented using `NumPy`⁴. The error tolerance of the integrator is set to $v_{tol} = 10^{-6}$.

C Linear stability of spatially uniform GTPase model

In this section we consider the steady states and their linear stability of equation (13).

¹ http://www.mathematik.uni-halle.de/wissenschaftliches_rechnen/forschung/software/

² <https://docs.scipy.org/doc/numpy-dev/f2py/>

³ <https://www.scipy.org/>

⁴ www.numpy.org

The Jacobian of the ODE system (13) at any steady state (L_{eq}, G_{eq}) is

$$J(L_{eq}, G_{eq}) = \begin{pmatrix} -\frac{2E}{\mu+2\eta} & \pm \frac{2F_{\max}}{\mu+2\eta} \frac{mG_c^m G_{eq}^{m-1}}{(G_c^m + G_{eq}^m)^2} \\ -\frac{G_T}{L_{eq}^2} \left(b + \gamma \frac{G_{eq}^n}{1+G_{eq}^n} \right) & \frac{\gamma n G_{eq}^{n-1}}{(G_{eq}^n + 1)^2} \left(\frac{G_T}{L_{eq}} - G_{eq} \right) - \left(b + I + \gamma \frac{G_{eq}^n}{1+G_{eq}^n} \right) \end{pmatrix}.$$

Model parameters are all positive, and $L_{eq}, G_{eq} > 0$ so in the Rac and Rho cases, respectively, the Jacobian has the sign patterns:

$$J_{\text{Rac}} = \begin{pmatrix} - & + \\ - & \text{sgn}(d) \end{pmatrix}, \quad J_{\text{Rho}} = \begin{pmatrix} - & - \\ - & \text{sgn}(d) \end{pmatrix}.$$

where

$$d := \frac{\gamma n G_{eq}^{n-1}}{(G_{eq}^n + 1)^2} \left(\frac{G_T}{L_{eq}} - G_{eq} \right) - \left(b + I + \gamma \frac{G_{eq}^n}{1+G_{eq}^n} \right).$$

Note that since $(L, G) \in \Delta$, where Δ is the invariant region in Result 1, we have that d is the difference of two positive numbers. It is straightforward to conclude the following (see for instance (Murray 1989)). In the Rho case, the steady states are either stable nodes or saddles and no oscillations are possible. In the Rac case the steady states are stable when $\text{sgn}(d) < 0$, and oscillations are possible when $\text{sgn}(d) > 0$.

C.1 Sharp-switch limit

Using a sharp-switch approximation we can easily compute two steady states:

1. When both nonlinear switches are off, i.e. $G \ll 1$, the steady states are:

$$L_{eq} = L_0, \quad G_1 = \frac{bG_T}{L_0(b+I)}.$$

Since the linearization of (13) is lower-triangular, the eigenvalues are readily found

$$\lambda_1 = \frac{-2E}{\mu+2\eta}, \quad \lambda_2 = -(b+I).$$

Since $b, I, E, \mu, \eta > 0$, we conclude that this steady state is a stable node. Finally, since $G_{eq} \ll 1$, we obtain an existence condition

$$G_T < L_0 \left(1 + \frac{I}{b} \right).$$

Therefore, the steady state of a large cell, with low total active GTPase can only exist if the total amount of GTPase is small.

2. In the case $G_c < G < 1$, i.e. one of the nonlinear switches is turned on, the steady states are:

$$L_{eq} = L_0 \pm \frac{F_{\max}}{E}, \quad G_2 = \frac{bG_T}{L_{eq}(b+I)}.$$

Since the linearization of (13) is lower-triangular as before, the eigenvalues are readily found

$$\lambda_1 = \frac{-2E}{\mu+2\eta}, \quad \lambda_2 = -(b+\gamma+I).$$

Since $b, I, \gamma, E, \mu, \eta > 0$, we conclude that this steady state is a stable node. A condition for the existence of this steady state is

$$\frac{L_0(b+\gamma+I)}{b+\gamma} < G_T < \frac{G_c L_0(b+\gamma+I)}{b+\gamma}.$$

Thus we must have some intermediate amount of GTPase.

3. In the case $1 < G < G_c$, i.e. one of the nonlinear switches is turned on, the steady states are:

$$L_{eq} = L_0, \quad G_2 = \frac{(b+\gamma)G_T}{L_0(b+\gamma+I)}$$

Eigenvalues are readily found, as before,

$$\lambda_1 = \frac{-2E}{\mu + 2\eta}, \quad \lambda_2 = -(b + \gamma + I).$$

From $b, I, \gamma, E, \mu, \eta > 0$ we conclude that this steady state is a stable node. The existence condition for this steady state can be written in either of two forms

$$\frac{L_0(b + \gamma + I)}{b + \gamma} < G_T < \frac{G_c L_0(b + \gamma + I)}{b + \gamma}, \quad \frac{L_0}{G_T - L_0} I - b < \gamma < \frac{L_0 G_c}{G_T - L_0 G_c} I - b.$$

For these ranges to be non-empty we require that $G_T > L_0 G_c$. Thus we must have some intermediate amount of GTPase.

4. In the case, when both nonlinear switches are turned on, i.e. $G \gg G_c$, the steady states are

$$L_{eq} = L_0 \pm \frac{F_M}{E}, \quad G_3 = \frac{(b + \gamma)G_T}{L_{eq}(b + \gamma + I)}.$$

Then the eigenvalues are

$$\lambda_1 = \frac{-2E}{\mu + 2\eta}, \quad \lambda_2 = -(b + \gamma + I).$$

Since $b, I, \gamma, E, \mu, \eta > 0$, this steady state is a stable node. The condition for existence of this steady state is given by

$$G_T > G_c L_{eq} \left(1 + \frac{I}{b + \gamma}\right), \quad \text{or} \quad \gamma > \frac{L_b G_c}{G_T - L_b G_c} I - b.$$

Thus only cells with a sufficiently amount of GTPase can be large or small.

In the bifurcation diagram of Fig. 8, the regions of existence of G_1, G_2 or G_3 are identified.

D The case of a deforming cell with conserved volume

Here we consider the case that the volume of a cell is roughly constant, while the cell deforms and its membrane size changed. This idea suggests a slight modification to our model. The modified mass conservation reads

$$G_T = G_i V + \beta G L,$$

where V is the constant volume of the cell, and β is a constant of proportionality with units of $[\text{length}]^2$. We can solve for G_i to get a relation analogous to (6):

$$G_i = \frac{G_T}{V} - \frac{\beta G L}{V}.$$

Notice that after substituting this into the well-mixed system, we can set $V = 1$ by rescaling b and γ . Therefore, we get

$$\frac{dG}{dt} = \left(b + \gamma \frac{G^n}{1 + G^n}\right) (G_T - \beta G L) - I G - G \left(\frac{\dot{L}}{L}\right). \quad (16)$$

This, together with (13a) and (13b), forms our new system.

Much of the analysis of this system is similar to the earlier case. The changes to the nullclines in the $G - L$ phase plane correspond to a vertical shift in the sharp switch limit, which can be compensated by adjusting the parameters. This suggests that the behaviors of the new system is similar to the original (13). The equilibrium branches and the conditions for their existence in the sharp switch limit are:

1. For $G \ll 1$:

$$L_{eq} = L_0, \quad G_{eq} = \frac{b G_T}{b \beta L_0 + I} \quad \text{exists provided} \quad G_T < \beta L_0 + \frac{I}{b}.$$

2. For $G_c < G < 1$:

$$L_{eq} = L_0 \pm \frac{F_{max}}{E}, \quad G_{eq} = \frac{b G_T}{b \beta L_{eq} + I} \quad \text{exists provided} \quad G_c \left(\beta L_{eq} + \frac{I}{b}\right) < G_T < \beta L_{eq} + \frac{I}{b}.$$

3. For $1 < G < G_c$:

$$L_{eq} = L_0, \quad G_{eq} = \frac{(b + \gamma) T}{(b + \gamma) \beta L_0 + I} \quad \text{exists provided} \quad \beta L_0 + \frac{I}{b + \gamma} < G_T < G_c \left(\beta L_0 + \frac{I}{b + \gamma}\right).$$

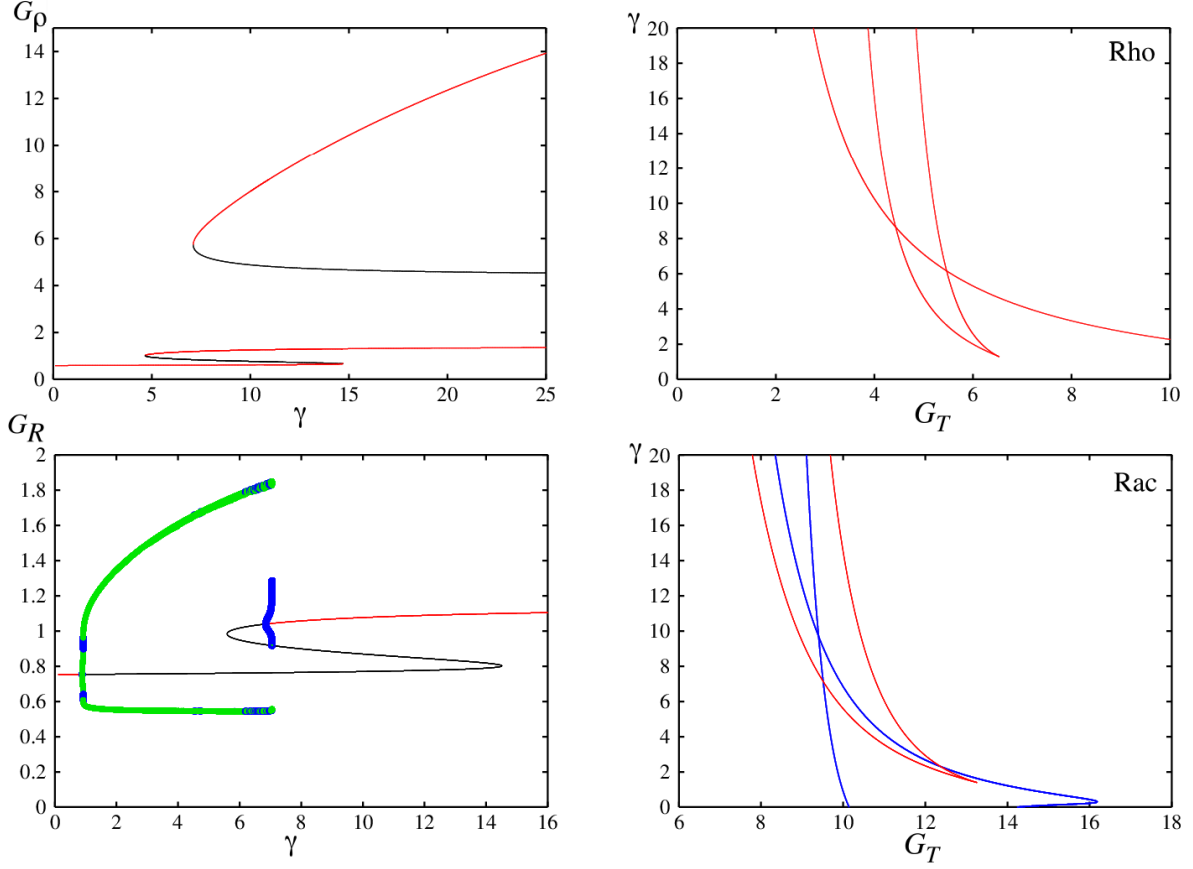


Fig. 11 Bifurcation diagrams as in Fig. 8, but for the constant volume spatially uniform GTPase model, (16). Top: the contractile (Rho) case, with parameters $k = 1, I = 5, L_0 = 3.5, \frac{2E}{\mu+2\eta} = 3, \frac{2F_{max}}{\mu+2\eta} = 10, G_c = 4, \beta = 1, G_T = 5, m = n = 10$. Bottom: the protrusive (Rac) case, with parameters $k = 1, I = 10, L_0 = 2.3, \frac{2E}{\mu+2\eta} = 8, \frac{2F_{max}}{\mu+2\eta} = 55, G_c = 0.9, \beta = 1, G_T = 10, n = 20, m = 10$. While the Rac case is still tristable, a fold point that previously connected the middle and high branch (in the original model) is now missing. These branches persist as $\gamma \rightarrow \infty$ whereas the lower branch exists only for low γ . In the Rac case, the Hopf curve in the two-parameter bifurcation diagram (lower right) differs significantly from the corresponding panel in Fig. 8, which yields parameter regimes where the limit cycle exists for $\gamma \rightarrow 0$.

4. For $G \gg G_c$:

$$L_{eq} = L_0 \pm \frac{F_{max}}{E}, G_{eq} = \frac{(b + \gamma)G_T}{(b + \gamma)\beta L_{eq} + I} \quad \text{exists provided} \quad G_T > G_c \left(\beta L_{eq} + \frac{I}{b + \gamma} \right).$$

In the Rho (contraction) case, tri-stability still occurs. In this model, we can more readily find parameter sets where the middle ($1 < G < G_c$) and high branch persist as $\gamma \rightarrow \infty$, whereas the low branch terminates at a fold point (Fig. 11). (This is also possible in the original model.) This suggests that even with a very large positive feedback in GTPase activity, and when GTPase activity is high enough to trigger that feedback, the cell can still stay at a large size. In contrast, in the original model, the regime where only the middle and high branch coexist is usually bounded above by some maximum γ , as seen in the regime labelled “2,3” in Fig. 8 (top right).

In the Rac (expansion) case, periodic orbits are still possible. The regime in which limit cycles exist is much wider than in the original model. We can identify parameter sets where a limit cycle exists even at $\gamma = 0$, which hints that in this model, a positive feedback in GTPase activity is not necessary for an oscillating cell.

Overall, the model variant with constant cell volume has the same regimes as the original model. However, the location and size of these regimes has shifted.

The Jacobian of the ODE system at a steady state (L_{eq}, G_{eq}) , is

$$J(L_{eq}, G_{eq}) = \begin{pmatrix} -\frac{2E}{\mu+2\eta} & \pm \frac{2F_{\max}}{\mu+2\eta} \frac{mG_c^m G_{eq}^{m-1}}{(G_c^m + G_{eq}^m)^2} \\ -\frac{2E}{\mu+2\eta} \frac{1}{L_{eq}} \frac{\gamma n G_T G^{n-1}}{(1+G^n)^2} - \beta L \left(b + \gamma \frac{G^n}{1+G^n} + G \right) - I \end{pmatrix}.$$

Model parameters are all positive, and $L_{eq}, G_{eq} > 0$ so in the Rac and Rho cases, respectively, the Jacobian has the sign patterns:

$$J_{\text{Rac}} = \begin{pmatrix} - & + \\ - & \text{sgn}(d) \end{pmatrix}, \quad J_{\text{Rho}} = \begin{pmatrix} - & - \\ - & \text{sgn}(d) \end{pmatrix}.$$

where

$$d := \frac{\gamma n G_T G^{n-1}}{(1+G^n)^2} - \beta L \left(b + \gamma \frac{G^n}{1+G^n} + G \right) - I.$$

The sign patterns are the same as in the original model, and thus the same conclusions apply.

References

- Bui J, Conway DE, Heise RL, Weinberg SH (2019) Mechanochemical coupling and junctional forces during collective cell migration. *bioRxiv* p 558452
- Camley BA, Zhao Y, Li B, Levine H, Rappel WJ (2013) Periodic migration in a physical model of cells on micropatterns. *Phys Rev Lett* 111(15):158102
- Crampin EJ, Gaffney EA, Maini PK (1999) Reaction and diffusion on growing domains: Scenarios for robust pattern formation. *B Math Bio* 61(6):1093–1120
- Cusceddu D, Edelstein-Keshet L, Mackenzie JA, Portet S, Madzvamuse A (2018) A coupled bulk-surface model for cell polarisation. *J Theor Biol*
- Dawes AT, Edelstein-Keshet L (2007) Phosphoinositides and rho proteins spatially regulate actin polymerization to initiate and maintain directed movement in a one-dimensional model of a motile cell. *Biophys J* 92(3):744–768
- Dierkes K, Sumi A, Solon J, Salbreux G (2014) Spontaneous oscillations of elastic contractile materials with turnover. *Phys Rev Lett* 113(14):148102
- Drasdo D, Höhme S (2005) A single-cell-based model of tumor growth in vitro: monolayers and spheroids. *Phys Biol* 2(3):133–47
- Gerisch A (2001) Numerical methods for the simulation of taxis diffusion reaction systems. Dissertation, Martin-Luther-Universität Halle-Wittenberg
- Holmes WR, Edelstein-Keshet L (2016) Analysis of a minimal rho-gtpase circuit regulating cell shape. *Phys Biol* 13(4):046001
- Holmes WR, Lin B, Levchenko A, Edelstein-Keshet L (2012) Modelling cell polarization driven by synthetic spatially graded rac activation. *PLoS Comput Bio* 8(6):e1002366
- Jilkine A, Edelstein-Keshet L (2011) A comparison of mathematical models for polarization of single eukaryotic cells in response to guided cues. *PLoS Comput Bio* 7(4):e1001121
- Liu Y (2019) Analysis of pattern formation in reaction-diffusion models for cell polarization. Master thesis, University of British Columbia
- Marée AF, Jilkine A, Dawes A, Grieneisen VA, Edelstein-Keshet L (2006) Polarization and movement of keratocytes: a multiscale modelling approach. *B Math Bio* 68(5):1169–1211
- Marée AF, Grieneisen VA, Edelstein-Keshet L (2012) How cells integrate complex stimuli: the effect of feedback from phosphoinositides and cell shape on cell polarization and motility. *PLoS Comput Bio* 8(3):e1002402
- Meinhardt H (1999) Orientation of chemotactic cells and growth cones: models and mechanisms. *J Cell Sci* 112(17):2867–2874
- Michaelson D, Silletti J, Murphy G, D'Eustachio P, Rush M, Philips MR (2001) Differential localization of rho gtpases in live cells: regulation by hypervariable regions and rhogdi binding. *J Cell Biol* 152(1):111–126
- Mori Y, Jilkine A, Edelstein-Keshet L (2008) Wave-pinning and cell polarity from a bistable reaction-diffusion system. *Biophys J* 94(9):3684–3697
- Mori Y, Jilkine A, Edelstein-Keshet L (2011) Asymptotic and bifurcation analysis of wave-pinning in a reaction-diffusion model for cell polarization. *SIAM J Appl Math* 71(4):1401–1427
- Murray JD (1989) *Mathematical Biology*. Springer, Berlin, Germany
- Neilson MP, Veltman DM, van Haastert PJ, Webb SD, Mackenzie JA, Insall RH (2011) Chemotaxis: a feedback-based computational model robustly predicts multiple aspects of real cell behaviour. *PLoS Biol* 9(5):e1000618
- Otsuji M, Ishihara S, Kaibuchi K, Mochizuki A, Kuroda S, et al. (2007) A mass conserved reaction-diffusion system captures properties of cell polarity. *PLoS Comput Bio* 3(6):e108
- Palsson E (2008) A 3-d model used to explore how cell adhesion and stiffness affect cell sorting and movement in multicellular systems. *J Theor Biol* 254(1):1–13

- Peyret G, Mueller R, d'Alessandro J, Begnaud S, Marcq P, Mege RM, Yeomans JM, Doostmohammadi A, Ladoux B (2019) Sustained oscillations of epithelial cell sheets. *Biophys J*
- Ryan GL, Watanabe N, Vavylonis D (2012) A review of models of fluctuating protrusion and retraction patterns at the leading edge of motile cells. *Cytoskeleton* 69(4):195–206
- Weiner R, Schmitt BA, Podhaisky H (1997) Rowmap—a row-code with krylov techniques for large stiff odes. *Appl Numer Math* 25:303–319
- Wolgemuth CW, Zajac M (2010) The moving boundary node method: a level set-based, finite volume algorithm with applications to cell motility. *J Comput Phys* 229(19):7287–7308
- Zehnder SM, Suaris M, Bellaire MM, Angelini TE (2015) Cell volume fluctuations in mdck monolayers. *Biophys J* 108(2):247–250
- Zmurchok C, Holmes WR (2019) Modeling cell shape diversity arising from complex rho gtpase dynamics. *bioRxiv* p 561373
- Zmurchok C, Bhaskar D, Edelstein-Keshet L (2018) Coupling mechanical tension and gtpase signaling to generate cell and tissue dynamics. *Phys Biol* 15(4):046004